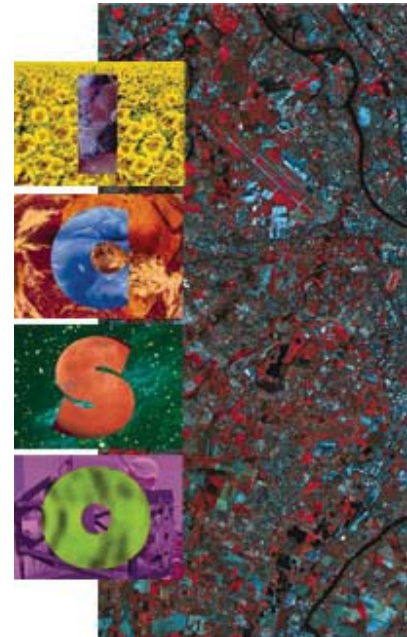


# International Conference on Space Optics—ICSO 2000

Toulouse Labège, France

5–7 December 2000

*Edited by George Otrio*



## *An effective procedure to operate tests of star tracker software routines using a sensor model*

*Giancarlo Rufino, Domenico Accardo*



**AN EFFECTIVE PROCEDURE  
TO OPERATE TESTS OF STAR TRACKER SOFTWARE ROUTINES  
USING A SENSOR MODEL**

**Giancarlo RUFINO**

*University of Naples Federico II – Dept. of Space Science and Engineering “Luigi G. Napolitano”  
Piazzale Tecchio 80, I-80125 Napoli, Italy – phone +39 0817682149, fax +39 0817682160,  
email rufino@unina.it*

**Domenico ACCARDO**

*Second University of Naples - Department of Aerospace Engineering  
via Roma 29, I-81031 Aversa (CE), Italy – phone +39 0817682149, fax +39 0817682160,  
email domenico.accardo@unina2.it*

**ABSTRACT** - *This paper presents a procedure for the validation of the software of an advanced star sensor by using a hardware model in a laboratory star field simulator. The mutual calibration of the sensor under test and of the simulator is realised by means of a neural network. It corrects errors from different sources adaptively, without need for specific models. Its correction capability has been compared to analytical models. Results of the procedure operation are presented to show that the angular measurement accuracy can be improved from 0.2° to 0.01°. Finally, its successful adoption for the validation of two star tracker software routines is reported.*

## 1 - INTRODUCTION

The present development of star trackers follows trends of different kind [BIRN 96, LIEB 95]. First, current budgetary limitations of space missions suggest that all the space equipment must change, so that overall mission costs decrease, including both development and operations. This has resulted in a great interest for small and micro satellites because the relevant launch cost greatly benefits from their low mass and small size. Hence, modern star trackers, as all on-board equipment, must be compact and have low mass and reduced power consumption. Another point is that the number of the on-board devices should be limited to the utmost. This can be accomplished by enhancing the functionality of single instruments and by introducing new, additional functions. Finally, the complexity of the on-board devices must be reduced in order that reliability is increased. Another aspect of the present development trends envisages that most of the functionality of a modern star tracker is realised by means of software routines [ESA 97]. Then, after a preliminary analysis of the operation requirements for the identification of adequate units and architecture, the hardware system and the software routines can be developed concurrently, reducing the time for project completion. Another great advantage of this strategy is that not only the enhancement of the already defined functionality, but also the introduction of new one can be achieved by only modifying the software under development. Nearly no impact results on the hardware section, if the maximum computational load is kept.

The adoption of the presently available commercial off-the-shelf components (COTS) seems to be feasible in this scenario [BIRN 96]. It offers several advantages: low cost, reliability, prompt availability. In addition, the present technology guarantees high performance also in COTS components, so that they are adequate for demanding applications, such as the space ones.

In this scenario, it is conceivable that hardware and software prototypal components are available at the same time. Besides independent validation of each component, such as computer simulations for the software, electrical tests of the data acquisition and processing units, or optics correct mounting verification, also end-to-end tests on the whole system can be operated already on the assembly of prototypal components. The validation of the interface adequacy can be performed, but also each single component can be tested in the nominal operating mode by means of ad hoc procedures. Such a kind of test configuration would allow for checking the complete system functionality, which is needed for preliminary prototypes, for the engineering models, and for flight units.

This work presents a procedure conceived to carry out the above tests on a star tracker in a laboratory facility that has been designed and realised to this purpose. The operation of the test procedure on a prototypal of the star tracker under development is reported in detail along with the obtained results, showing the validity of system and of the procedure. This activity takes place in the framework of a project for the design and the realisation of a low-cost, fully autonomous star tracker, which is being carried out in co-operation at the two universities of Naples.

## 2 - OBJECTIVES

The sensor routines to be tested produce the attitude measures required in different mission phases (attitude angles and/or rates) at different accuracy by means of various techniques. Distinct procedures are needed along with a supervising control logic that manages their operation and also adapts the hardware acquisition mode to running conditions. The primary objectives here considered for the tests are the validation of the techniques, of their implementation, of the logic for their management and timing, and of the robustness of the software system. The input data to all the routines of a modern autonomous star tracker consist in measured positions and brightness of several stars in the sensor field-of-view (FOV) and/or of the angular separations between them. Additional features could require the same measurements, but relevant to non-stellar objects for extended tracking operation. Hence, the tests of interest basically need that sensor acquisitions extending over the whole FOV are processed. The control logic essentially works on the basis of the estimate of the platform dynamics given by the measurement routines. Its validation can be obtained by running tests during which the input data of the routines change over a medium-long span of time as resulting from varying dynamical conditions of the platform.

Another point, assumed as primary requirement for the test procedure, is the validation of sensors not yet calibrated for angular measurements. This is very important with respect to the reduction of development cost and time.

To carry out reliable validation, realistic star field frames must be processed, since this is the kind of images acquired during nominal operation. In addition, aiming at the assessment of the system robustness, tests accounting for perturbations, such as platform vibrations, partial FOV occultation, and observation of non stellar objects, must be planned.

The described procedure is relevant to a particular strategy of operating these tests. It consists in the simulation of realistic star field scenes to be acquired and processed. It has been preferred to simulating the frames acquired by the sensor because it offers several advantages:

- i) end-to-end tests are operated, including all the subsystems of the sensor, both hardware and software;
- ii) inaccurate modelling of component is avoided, thus increasing test reliability;
- iii) preliminary prototypal models as well as flight units can be tested without introducing ad hoc input interfaces.

The star field scene simulation is based on a high-resolution cathode ray tube (CRT) display controlled by a personal computer. It is briefly described in the following section. Realistic star field scenes can be generated, single or in sequence to reproduce particular manoeuvres, also

introducing perturbations. The attainable simulation performance makes the routine suitable for medium-accuracy calibration of the sensor, which allows for the validation of its software-based functionality, as shown by the reported applications.

### 3 - EMPLOYED HARDWARE

The procedure has been conceived to be operated in the laboratory facility specifically designed for these tests. The arrangement of the facility components is shown in fig. 1. It is based on a 21" high-resolution CRT display, which is controlled by an Intel Pentium II 450 MHz personal computer thanks to an AGP video card endowed with 8 MB memory. Simulated star field scenes are displayed on the 21" display, while an additional low-resolution display, connected to another video card, shows the controls in Windows<sup>TM</sup> based environment. A collimating optics is adopted in order that the scene displayed by the CRT display appears as if at infinite distance from the sensor location. The collimator focal length  $f_c$  is selected so that the CRT screen covers the whole sensor FOV.

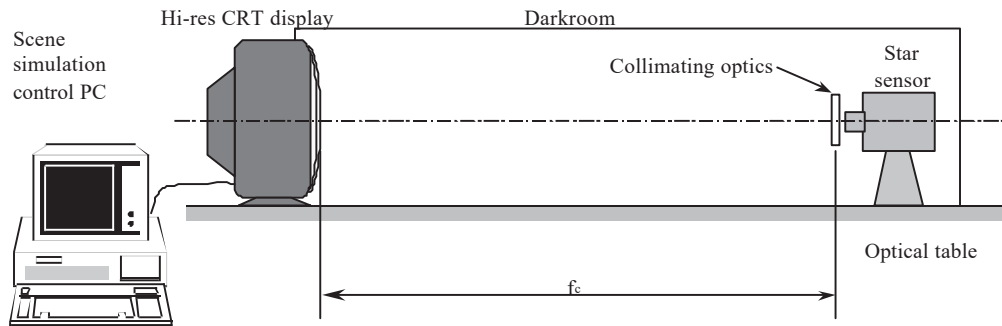


**Fig. 1:** sketch of laboratory star field simulation facility.

Single stars in the scene are simulated by addressing single pixels on the CRT display. Its resolution determines the accuracy of the star field simulation. In particular, its dot pitch  $d_{\text{pix}} = 0.26$  mm gives the minimum angular separation between adjacent positions  $\delta_{\text{pix}}$  as

$$\delta_{\text{pix}} = 2 \tan^{-1} \frac{d_{\text{pix}}/2}{f_c} \quad (3.1)$$

Then, the maximum angular error resulting from star position approximation at pixel location is  $\pm\delta_{\text{pix}}/2$ . The star apparent visual magnitude can also be simulated in the range 0-7 thanks to the CRT maximum luminance of 25 fL and it can be controlled over 256 digital counts of pixel brightness. Finally, also star colour can be accounted for by modifying the ratio between the red, green, and blue pixel colour components.

The installation of sensor to be tested in the facility is realised by means a series of translation and rotation stages, which allow for the adjustment of position and orientation of the instrument with respect to the CRT screen. Besides large-scale displacements, also micrometric fine tuning is available.

Presently the laboratory facility has been tuned for operation with the sensor under development (fig. 2) [RUOC 99]. The unit has been realised using COTS components. The image forming subsystem is the one at the most prototypal stage. Presently, a symmetrical combination of two plano-convex lenses has been adopted to obtain the required focal length for adequate FOV aperture [ACCA 00a]. This configuration has been selected to minimise symmetrical and non-symmetrical aberrations. The image acquisition subsystem is based on the interline-transfer charge coupled device (CCD) photodetector ICX039DLA by Sony and on the related control electronics. Acquired



Fig. 2: star sensor prototype.

Field of view [Horizontal x Vertical] (°)	15.4 x 13
Effective focal length (mm)	27
F-number	1.2
Image sensor	½-inch interline transfer CCD
Image size [Horizontal x Vertical] (pixels)	768 x 576
Instantaneous field of view (°)	0.018 x 0.017

Tab. 1: main characteristics of the star tracker under development.

frames are encoded in CCIR standard video format and outputted to a personal computer endowed with a frame grabber card. This computer performs the processing and the relevant routines are developed in high level languages. Angular resolution better than the sensor instantaneous FOV is achieved by applying the hyperacuity technique to slightly defocused images [LIEB 95].

The sensor main characteristics are in tab. 1. The FOV aperture size drives the choice of  $f = 1.4$  m, so that the sensor can be correctly installed in the laboratory facility. The resulting main simulation performance is reported in tab. 2. It is worth noting that the apparent angular separation between adjacent pixels of  $0.013^\circ$  causes an average inaccuracy in the position of single stars in the simulated star field scene in the order of  $0.007^\circ$ .

Angular size of the CRT display area (°)	16.5 x 12.4
Apparent angular diameter of a single CRT pixel at screen center (°)	0.014
Angular separation between adjacent pixels [horizontal or vertical / diagonal direction] (°)	0.011 / 0.015

Tab. 2: main features of the test system in combination with the sensor under development.

#### 4 – PROCEDURE

The mutual calibration of the star sensor under test and of the indoor star field simulator must be performed, since several assumptions at the basis of the routine for star field scene simulation are not fully realised. They are:

- the CRT screen is flat and its pixel spacing is exactly known;
- the optics are modelled as a perfect imaging system [WALD 93] and the CCD is flat and co-axially mounted;
- when the sensor under test is installed in the test facility, its boresight axis is perpendicular to the CRT in its centre and the horizontal (H) and vertical (V) reference directions in the two systems are coincident.

This can not be realised at the required accuracy by installing the model in the test facility after simply assuming mechanical references for mounting. Indeed, an initial rough manual alignment is made using the translation and rotation stages. Two different characteristics of the acquired images are considered. It is required that the central pixel of the CRT screen is imaged at the center of the CCD and that the symmetry of the scenes displayed by the CRT screen is kept. The former task is accomplished by means of the centroiding algorithm, which is also operated during the star tracking. The latter is realized by examining orientation and symmetry characteristics of a uniformly spaced grid of bright points displayed by the CRT. At this stage, the alignment is still unsatisfactory. As shown in the following section, image position and angular measurements operated by the sensor result in non negligible deviations from the values assumed at the stage of scene simulation.

The further adjustment is introduced via a software procedure by constructing a two-dimensional correction of the raw measurements of the sensor, which is described in the following. It aims at compensating the residual geometric misalignment of the model in the test facility, but also incorrect assumptions on the observation geometry made at the stage of scene simulation, incorrect modelling of the simulated scene (display shape and orientation, pixel spacing, etc.), optics aberration effects.

Firstly, a set of 567 uniformly distributed pixels is displayed in sequence to the sensor. They are arranged in 21 rows and 27 columns and are evenly spaced to form a regular grid. Grid spacing has been selected to correct only low spatial frequency errors. It is worth noting that the sub-pixel errors affecting the centroiding algorithm [BIRN 96, BORG 94] can not be corrected by the network. The relevant centroid positions are acquired and stored in memory.

The second step of the procedure consists in the training of a back-propagation neural network to perform the mapping of the correction. Since some of the errors to be corrected have non-linear dependence on the FOV position, such as the aberrations introduced by the lenses, more than one hidden-layer of processing elements is needed. In fact, the Kolmogorov theorem [HAGA 96] states that back-propagation neural networks can achieve non-linear mapping only if they have at least two hidden-layers of processing elements. For the adopted neural network, three hidden-layers with ten processing elements have been chosen. The number of processing elements has been slightly overdimensioned, in order to minimise network convergence time and to improve the capability of the network to generalise the mapping. Indeed, an increase in the number of processing elements "smoothens" the mapping function and reduces the error in points not in the training set. The sigmoid function has been selected as transfer function for the hidden layers and the linear function for the output layer as suggested for nominal network adoption [HAGA 96]. The training has been realised using the Neural Network Toolbox of Matlab<sup>®</sup> [DEMU 92].

Finally, the network has to be validated verifying if its performance in points not included in the training set is acceptable for considered applications.

## 5 - VALIDATION AND ANALYSIS OF THE CORRECTION

The neural network has been trained for 100 epochs before evaluating its performance. A training epoch is the processing of the whole set of examples by the learning routine for weights assessment. The learning curve in fig. 3 shows that the target correction performance has been almost met after 25 epochs. The final residual mean square correction error is in the order of  $7 \times 10^{-12}$  meters.

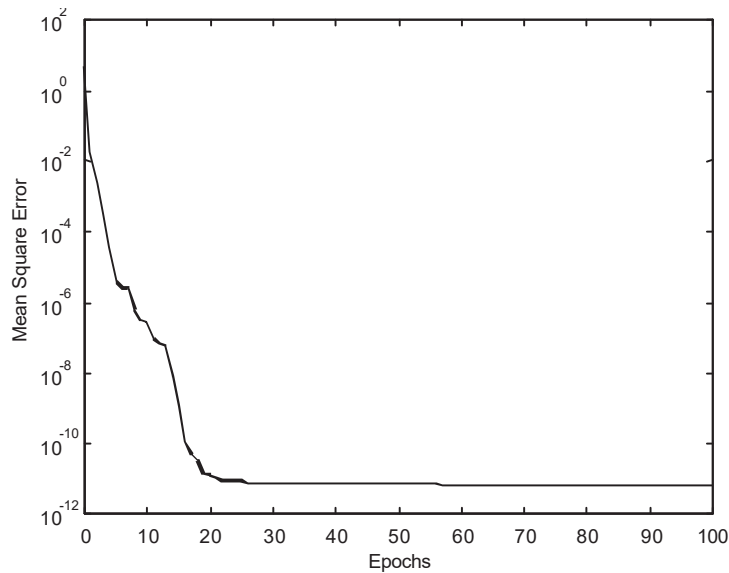


**Fig. 3:** neural network learning curve.

After the completion of the training process, the neural network has been operated on a set of 520 test points, arranged in 20 rows and 26 columns. It has been formed in the same way as the training set, but, in this case, the reference locations have been selected in the middle of the training grid. This kind of choice allows for the evaluation of the network capability to generalise its results, since the test points are uniformly distributed and at the largest possible distance from the training points.

In Tab.3 the errors in image position and angular measurement are reported, assuming a perfect alignment of the model and without

introducing the neural correction. In particular, the error in angular separation is shown in the table using two different parameters. The first parameter is the difference in the angular separations from the boresight of the observed centroids and of the assigned positions (second row), which characterises the accuracy in measurement of angular separations because it depends on the orientation of the misplacement vector. Differently, the third row contains the angular separation between the observed positions and the relevant assigned ones, which estimates the accuracy attainable in apparent position measurements. Hence, this feature can be linked to the attitude determination accuracy.

	mean	std
Displacement (m)	$5.40 \times 10^{-5}$	$3.12 \times 10^{-5}$
Error in the angle with boresight (°)	$2.57 \times 10^{-2}$	$7.24 \times 10^{-2}$
Angular displacement (°)	$1.14 \times 10^{-1}$	$6.56 \times 10^{-2}$

**Tab. 3:** statistics of the error before the neural network correction.

Tab. 4 shows the same errors as in Tab. 3 calculated for the test points after the correction operated by the neural network. By comparing the results obtained in the two cases it can be observed that the network has introduced an improvement of one order of magnitude in the evaluation of the angular positions and separations. In fact, the errors reported before the correction are in the order of  $0.1^\circ$ , whereas they are in the order of  $0.01^\circ$  after the correction.

	Mean	Std
Displacement (m)	$5.59 \times 10^{-6}$	$3.66 \times 10^{-6}$
Error in the angle with boresight (°)	$-2.16 \times 10^{-5}$	$1.04 \times 10^{-2}$
Angular displacement (°)	$1.18 \times 10^{-2}$	$7.71 \times 10^{-3}$

**Tab. 4:** statistics of the residual error after the neural network correction.

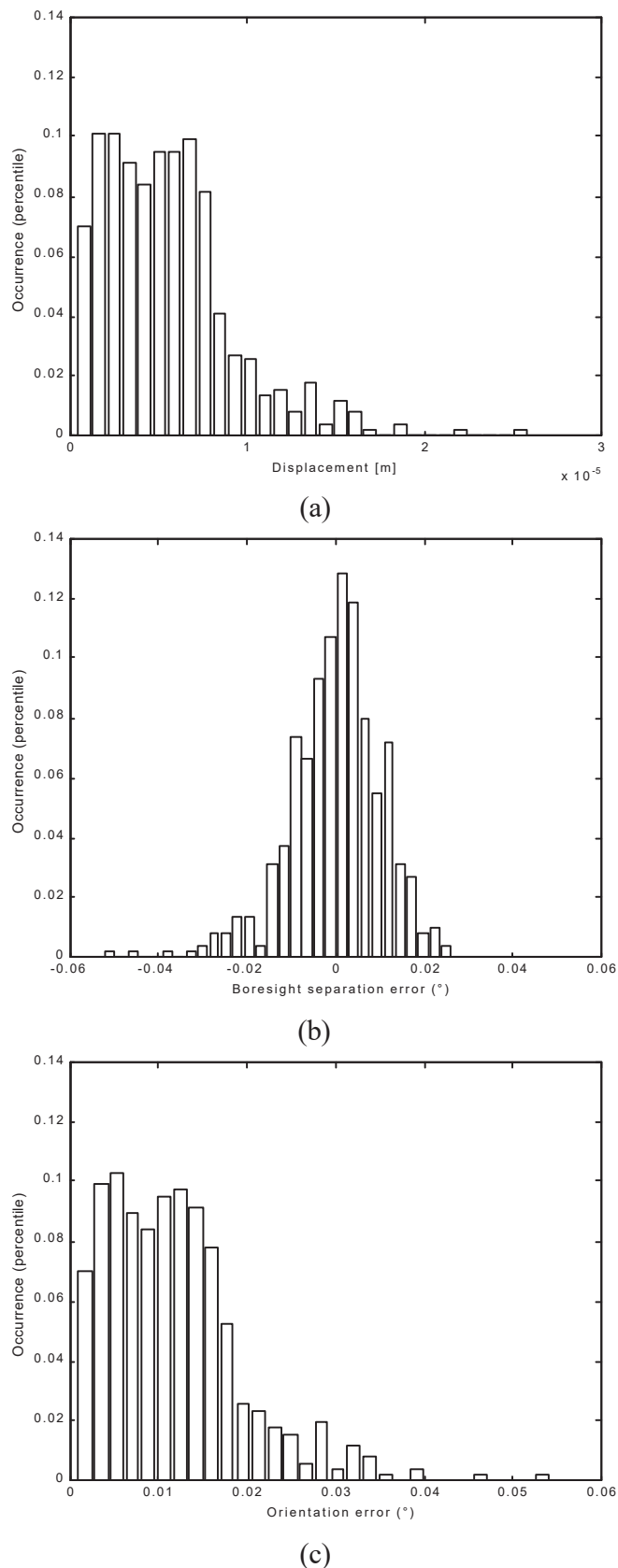


**Fig. 4:** distribution of the residual error after neural network correction: star position determination (a), angular separation from boresight (b), and orientation of single star line of sight (c).

Fig. 4 shows the distributions relevant to the statistics of Tab.4. These errors are in agreement with the inaccuracy resulting from the sum of the monitor pixel spacing error ( $0.007^\circ$ ) and the centroiding error. The initial misalignment introduces an error not acceptable for star tracking applications but, after network correction, the attained accuracy allows for application to tracking simulation using the apparatus.

The obtained image position correction, which is plotted in fig. 5, has been analysed. It has been compared to a model capable of accounting only for rigid rotation and reference axes scaling:

$$\begin{aligned} x_m &= A x_r + B y_r \\ y_m &= -B x_r + C y_r \end{aligned} \quad (5.1)$$

where  $x_m$  and  $y_m$  [ $x_r$  and  $y_r$ ] are the model-corrected coordinates [the observed coordinates] in the image. Two different scale factors have been envisaged for H and V directions. This is to compensate optics aberrations, missed parallelism of simulation screen and image plane, and incorrect CRT display modelling (in particular, different errors in the H and V pixel spacings). Shift of the reference frame origin has not been introduced, since it is not necessary after making the CRT and CCD centres match. The coefficient of the transformation have been computed to get the least-square (LSQ) best-fit of the model (5.1) in the reference grid points. In the case of the two applications considered in the next section, the result is  $A=1.14$ ,  $B=0.00837$ , and  $C=1.20$ , i.e., the model introduces an axis scale correction in the order of 14% and 20% on the H and V axes, respectively, and a rotation of  $\sin^{-1}(C) \approx 0.48^\circ$ .

Fig. 6 sketches the relevant scaling and rotation displacements, respectively. Being the latter very small, they have been magnified 10 times. Fig. 7 shows the residuals of the correction law on the reference points. Also these data have been magnified in the plot, adopting a factor 100 due to their very low order of magnitude. Basically, they correct missed parallelism of scene and image planes. Tab. 5 reports the

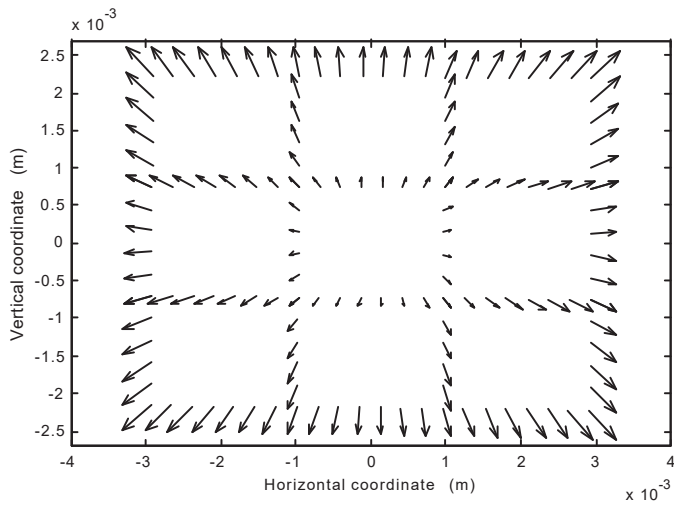
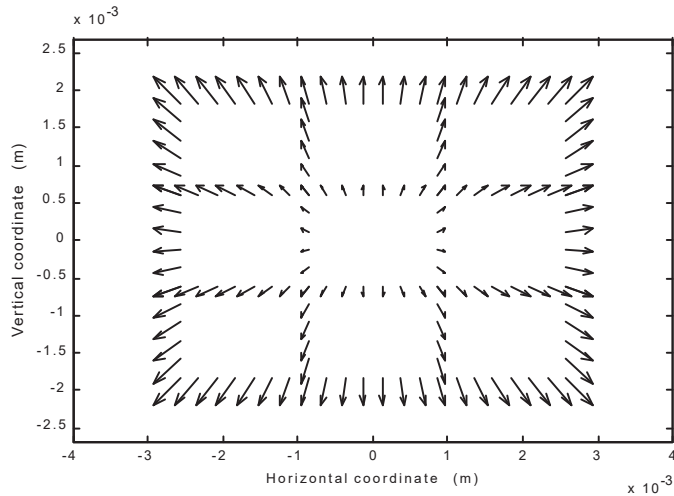
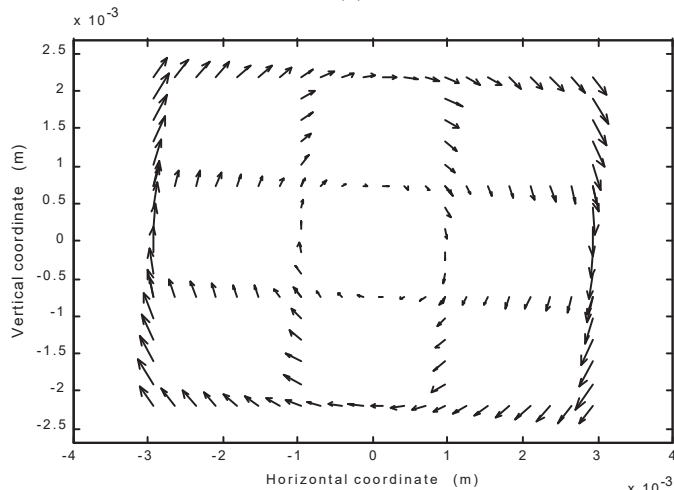


**Fig. 5:** neural network correction of imaged coordinates.



(a)



(b)

**Fig. 6:** LSQ correction model: axes scaling (a) and rotation (b) components. Scaling displacements are in scale, rotation ones are magnified 10 times.

deviation of this LSQ linear correction from the reference grid point positions. The attained performance is worse than the one of the neural network. This means that an adequate correction can be performed only by using an analytical model that is more complex than the one in (5.1), thus confirming the validity of the choice of a neural network. Moreover, the high-quality results of the latter are obtained by means of an intrinsically adaptive tool without any preliminary modelling of the problem, which avoids errors due to incorrect problem analysis.

## 6 - EXAMPLES OF APPLICATION AND RESULTS

In this section two examples of application for the mutual calibration procedure are discussed, which proves the capability of the routine to provide accuracy in star position determination adequate for star tracking.

The first example is the application of the initial acquisition routine discussed in details in [ACCA 00a]. Initial acquisition is the operative mode supported by autonomous star sensors that allows for real-time first attitude determination based only on the observed star field, without any additional input, in particular from other attitude sensors. A series of 1000 star field scenes have been presented to the sensor model. The routine succeeded in identifying the star field scene in 96.0% of cases and the misidentification percentage has been only 0.2%. The total non misleading output percentage has been 99.8% because acquisition failures do not input erroneous data to the attitude control system. The identified attitude is expressed by means of the Euler angles, which give the rigid rotation between of the sensor fixed reference frame and the inertial reference frame. This angles are computed using the measured positions of two identified stars. The results are in Tab. 6. Their value is fully compliant with the requirement of the European Space Agency for the initial acquisition [ESA 97].

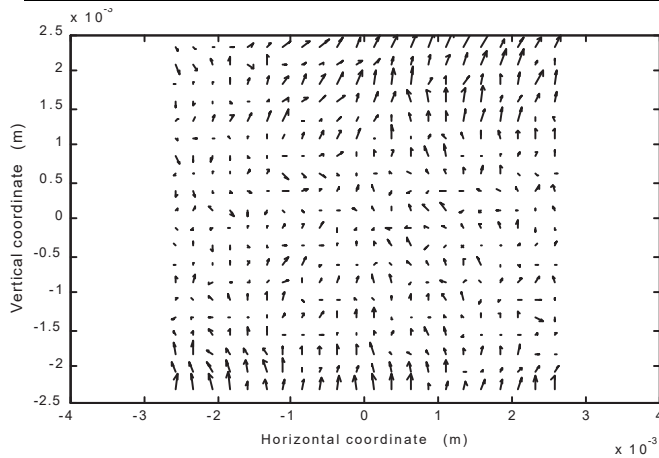


**Fig. 7:** residuals of the LSQ correction in the points of the training set. A magnification factor of 100 has been adopted in the plot.

	Mean	Std
Displacement $r$ (m)	$8.14 \times 10^{-6}$	$5.18 \times 10^{-6}$
Error in the angle with boresight ( $^{\circ}$ )	$-5.79 \times 10^{-5}$	$1.62 \times 10^{-2}$
Angular displacement ( $^{\circ}$ )	$1.72 \times 10^{-2}$	$1.09 \times 10^{-2}$

**Tab. 5.** Statistics of the residual error after the linear least-square correction.

	Computed angle errors	
	Mean	Std
1 <sup>st</sup> Euler angle ( $^{\circ}$ )	$2.0 \times 10^{-2}$	$4.0 \times 10^{-2}$
2 <sup>nd</sup> Euler angle ( $^{\circ}$ )	$1.2 \times 10^{-2}$	$1.8 \times 10^{-2}$
3 <sup>rd</sup> Euler angle ( $^{\circ}$ )	$1.5 \times 10^{-1}$	$3.5 \times 10^{-1}$
Boresight axis pointing ( $^{\circ}$ )	$1.9 \times 10^{-2}$	$1.4 \times 10^{-2}$

**Tab. 6:** Accuracy of initial attitude reconstruction (example 1).

	Computed solution error	
	Mean	Std
$x$ ( $^{\circ}/s$ )	$3.0 \times 10^{-3}$	0.13
$y$ ( $^{\circ}/s$ )	$1.8 \times 10^{-2}$	0.29
$z$ ( $^{\circ}/s$ )	$-3.3 \times 10^{-3}$	1.01
$ \dot{u} $ ( $^{\circ}/s$ )	$1.2 \times 10^{-2}$	0.58
Angular deviation ( $^{\circ}$ )	5.7	8.6

**Tab. 7:** Accuracy of angular velocity estimation (example 2).

## 7 - CONCLUSIONS

A procedure to carry out laboratory tests on hardware models of modern star sensors has been presented. The primary objective is the operation of end-to-end tests to validate the functionality of the complete system, including all hardware components and software routines, even using prototypes and, possibly, prior to fine calibration. In particular, the major interest is in validating the

The second example is a routine for the computation of the body fixed components of the angular velocity vector  $\dot{u}$  during fast-rotation phases ( $2-10^{\circ}/s$ ). In these conditions the stars are imaged by the sensor as elongated stripes rather than isolated spots. The complete presentation of the routine is in [ACCA 00b]. The relevant results are shown in Tab. 7 ( $x$ ,  $y$  and  $z$  are the searched components in the body reference frame  $xyz$ ). Also in this case the results are in accordance with the requirements reported in [ESA 97].

sensor functionality based on software routines. The described procedure has been conceived to meet these requirements when the acquisition of simulated star field scenes in a laboratory facility is envisaged. In this case, only the mutual calibration of the sensor and of the star field simulator guarantees correct tests. Adequate agreement between observed and simulated star positions must be realised. This has been achieved by introducing a neural network based correction. The neural approach has been chosen because it is intrinsically adaptive, which is a great advantage when an satisfactory correction model is not feasible. This is the case of interest, where errors have sources of various kind and distinct contributions cannot be adequately modelled. In addition, the procedure operation efficiency allows repeated test campaigns. The residual angular error is in the order of  $0.01^\circ$ , which is definitely suitable for testing star tracker software routines, as shown in the two presented successful applications. Furthermore, the use of the procedure can be extended. The procedure operation on a system calibrated for static angular measurements allows for the assessment of the dynamical measurement accuracy. The same strategy of a neural correction law can also be adopted for fine angular calibration of the sensor, to be carried out by using high-accuracy laboratory instrumentation. Finally, an analogous approach can be chosen for in-flight re-calibration of operating units.

## REFERENCES

- [BIRN 96] M. M. Birnbaum: "Spacecraft Attitude Control Using Star Field Trackers", *Acta Astronautica*, Vol. 39, No. 9-12, 1996, pp. 763-773.
- [LIEB 95] C. C. Liebe: "Star Trackers for Attitude Determination", *IEEE Aerospace and Electronic Systems Magazine*, Vol. 10, No. 6, pp. 10-16, 1995.
- [ESA 97] "Work Statement for the Study on Autonomous Star Tracker Algorithms", *ESA Document WSC-97-WS-AST*, 1997.
- [RUOC 99] C. Ruocchio, D. Accardo, G. Rufino, S. Mattei, and A. Moccia: "Development and Testing of a Fully Autonomous Star Tracker", *Digest of the 2<sup>nd</sup> International Symposium of the IAA on Small Satellites for Earth Observation*, Berlin, Germany, 12-16 April 1999, pp. 285-288.
- [ACCA 00a] D. Accardo and G. Rufino: "Innovative Solution for Initial Acquisition by an Autonomous Star Sensor: Algorithm, Implementation, and Test," *Proceedings of the 7<sup>th</sup> Saint Petersburg International Conference on Integrated Navigation Systems*, Saint Petersburg, Russia, 29-31 May 2000, pp. 28-37.
- [WALD 93] G. Waldman and J. Wootton: *Electro-Optical Systems Performance Modeling*, Artech House Inc., Norwood, MA, USA, 1993.
- [BORG 94] G. Borghi, D. Procopio, M. Magnani, S. Pieri, and S. Becucci: "Stellar Reference Unit for CASSINI Mission", *Proceedings SPIE*, Vol. 2210, p. 150-161, 1994.
- [HAGA 96] M.T. Hagan, H.B. Demuth, and M. Beale: *Neural Network Design*, PWS Publishing Company, Boston, MA, USA, 1996.
- [DEMU 92] H. Demuth and M. Bale: *Neural Network Toolbox for Use with MATLAB<sup>®</sup>*, The Math Works Inc., Natick, MA, USA, 1992.
- [ACCA 00b] D. Accardo and G. Rufino: "A Procedure for Three-Dimensional Angular Velocity Determination Using a Star Sensor in High-Rate Rotation Modes," *presented at the 51<sup>st</sup> International Astronautical Congress, Rio de Janeiro, Brazil, 2-6 October 2000*, paper IAF-00-A.2.03.